

DOI: 10.1002/cbic.201402000

# In Vivo Structure–Activity Relationship Studies Support Allosteric Targeting of a Dual Specificity Phosphatase

Vasiliy N. Korotchenko,<sup>[a, f]</sup> Manush Saydmohammed,<sup>[b]</sup> Laura L. Vollmer,<sup>[c]</sup> Ahmet Bakan,<sup>[d]</sup> Kyle Sheetz,<sup>[b]</sup> Karl T. Debiec,<sup>[e]</sup> Kristina A. Greene,<sup>[e]</sup> Christine S. Agliori,<sup>[e]</sup> Ivet Bahar,<sup>[d]</sup> Billy W. Day,<sup>[a, c, e]</sup> Andreas Vogt,<sup>\*[c, d]</sup> and Michael Tsang<sup>\*[b]</sup>

Dual specificity phosphatase 6 (DUSP6) functions as a feedback attenuator of fibroblast growth factor signaling during development. In vitro high throughput chemical screening attempts to discover DUSP6 inhibitors have yielded limited success. However, in vivo whole-organism screens of zebrafish identified compound **1** (BCI) as an allosteric inhibitor of DUSP6. Here we designed and synthesized a panel of analogues to define the structure–activity relationship (SAR) of DUSP6 inhibition. In

vivo high-content analysis in transgenic zebrafish, coupled with cell-based chemical complementation assays, identified structural features of the pharmacophore of **1** that were essential for biological activity. In vitro assays of DUSP hyperactivation corroborated the results from in vivo and cellular SAR. The results reinforce the notion that DUSPs are druggable through allosteric mechanisms and illustrate the utility of zebrafish as a model organism for in vivo SAR analyses.

## Introduction

Dual specificity phosphatases (DUSPs) represent a family of enzymes that catalyze the dephosphorylation of proteins on both phosphotyrosine and phosphoserine/phosphothreonine residues within the same substrate. DUSP6, also known as mitogen-activated protein kinase phosphatase 3 (MKP3), belongs to a subgroup of eleven dual specificity phosphatases that dephosphorylate and inactivate mitogen-activated protein kinases (MAPKs).<sup>[1–3]</sup> During development, DUSP6 functions as a negative feedback regulator of fibroblast growth factor (FGF) signaling.<sup>[4–6]</sup> The discovery of potent and selective inhibitors of dual specificity phosphatases has been hindered by a high

degree of conservation between the DUSP active sites and their shallow and feature-poor topology.<sup>[1]</sup> In addition, the presence of a reactive, active site cysteine, which is critical for enzymatic activity but displays high nucleophilicity and sensitivity to oxidation, due to a low pK<sub>a</sub> sulfhydryl moiety, has hampered drug discovery efforts.<sup>[7]</sup> Perhaps not too surprisingly, in vitro screens for DUSP inhibitors have yielded hit compounds that were redox reactive,<sup>[8]</sup> lacked in vivo activity,<sup>[9]</sup> or had activities not readily reconciled with DUSP inhibition.<sup>[10]</sup>

The advent of a whole organism live reporter for FGF activity (*Tg(dusp6:EGFP)<sup>pt6</sup>*)<sup>[11,12]</sup> enabled the discovery of a biologically active inhibitor of zebrafish DUSP6, (*E*)-2-benzylidene-3-(cyclohexylamino)-2,3-dihydro-1*H*-inden-1-one (BCI), designated here as **1**.<sup>[13]</sup> Chemical complementation assays revealed that **1** specifically inhibited DUSP6 and DUSP1, but not the related DUSP5.<sup>[13]</sup> Interestingly, **1** lacked antiphosphatase activity in a traditional biochemical assay with bacterially produced recombinant protein and therefore was missed in prior in vitro screens for DUSP inhibitors.<sup>[14]</sup> Instead, **1** selectively inhibited DUSP activity in the presence of ERK, which activates DUSP6 through a conformational change that brings a general acid residue within close proximity to the active site cysteine, enhancing its nucleophilicity.<sup>[15]</sup> The zebrafish system therefore captured the inhibitory activity of **1** against the biologically relevant phosphatase activity of DUSPs and provided a useful chemical probe to study the role of DUSP6 in embryonic development and adult immunity.<sup>[13,16–21]</sup>

To explore structure–activity relationship (SAR) of **1** and DUSP6 inhibition, we synthesized a series of 29 analogues with modifications in four functional groups of the **1** pharmacophore. SAR was evaluated for FGF hyperactivation in vivo by using transgenic zebrafish that report on FGF activity<sup>[11]</sup> and for DUSP6 and DUSP1 inhibition in cell-based chemical comple-

[a] V. N. Korotchenko,<sup>+</sup> B. W. Day  
Department of Pharmaceutical Sciences, University of Pittsburgh  
3501 Fifth Avenue, Pittsburgh, PA 15213 (USA)

[b] M. Saydmohammed,<sup>+</sup> K. Sheetz, M. Tsang  
Department of Developmental Biology, University of Pittsburgh  
3501 Fifth Avenue, Pittsburgh, PA 15213 (USA)  
E-mail: tsang@pitt.edu

[c] L. L. Vollmer, B. W. Day, A. Vogt  
The University of Pittsburgh Drug Discovery Institute  
University of Pittsburgh  
3501 Fifth Avenue, Pittsburgh, PA 15213 (USA)  
E-mail: avogt@pitt.edu

[d] A. Bakan, I. Bahar, A. Vogt  
Department of Computational & Systems Biology, University of Pittsburgh  
3501 Fifth Avenue, Pittsburgh, PA 15213 (USA)

[e] K. T. Debiec, K. A. Greene, C. S. Agliori, B. W. Day  
Department of Chemistry, University of Pittsburgh  
3501 Terrace Street, Pittsburgh, PA 15213 (USA)

[f] V. N. Korotchenko<sup>+</sup>  
Present address: Walter Reed Army Institute of Research  
503 Forney Drive, Silver Spring, MD 20910 (USA)

[<sup>+</sup>] These authors contributed equally to this work.

 Supporting information for this article is available on the WWW under <http://dx.doi.org/10.1002/cbic.201402000>.

mentation assays.<sup>[13]</sup> These SAR studies revealed a strong correlation between *in vivo* FGF hyperactivation and inhibition of cellular DUSPs and a lack of correlation between biological activity and whole organism toxicity. Biochemical assays for substrate-induced DUSP6 hyperactivation corroborated the inhibitory activities of the new analogues.

The selective inhibition of substrate-induced DUSP6 activation by **1** was reconciled by molecular modeling studies of the 1–DUSP6 interaction. Unbiased docking simulations supported that **1** would bind to the low-activity form of DUSP6, occupying a novel allosteric binding site adjacent to the phosphatase active site.<sup>[13]</sup> Refined scoring of potential docking modes by using Poisson–Boltzmann surface area (PBSA) binding free-energy calculations indicated a preferred binding orientation for **1**, in which its cyclohexylamino side chain and  $\alpha,\beta$ -unsaturated ketone moiety form hydrogen bonds with DUSP6. Collectively, these results support the hypothesis that DUSPs can be targeted through allosteric mechanisms.

## Results

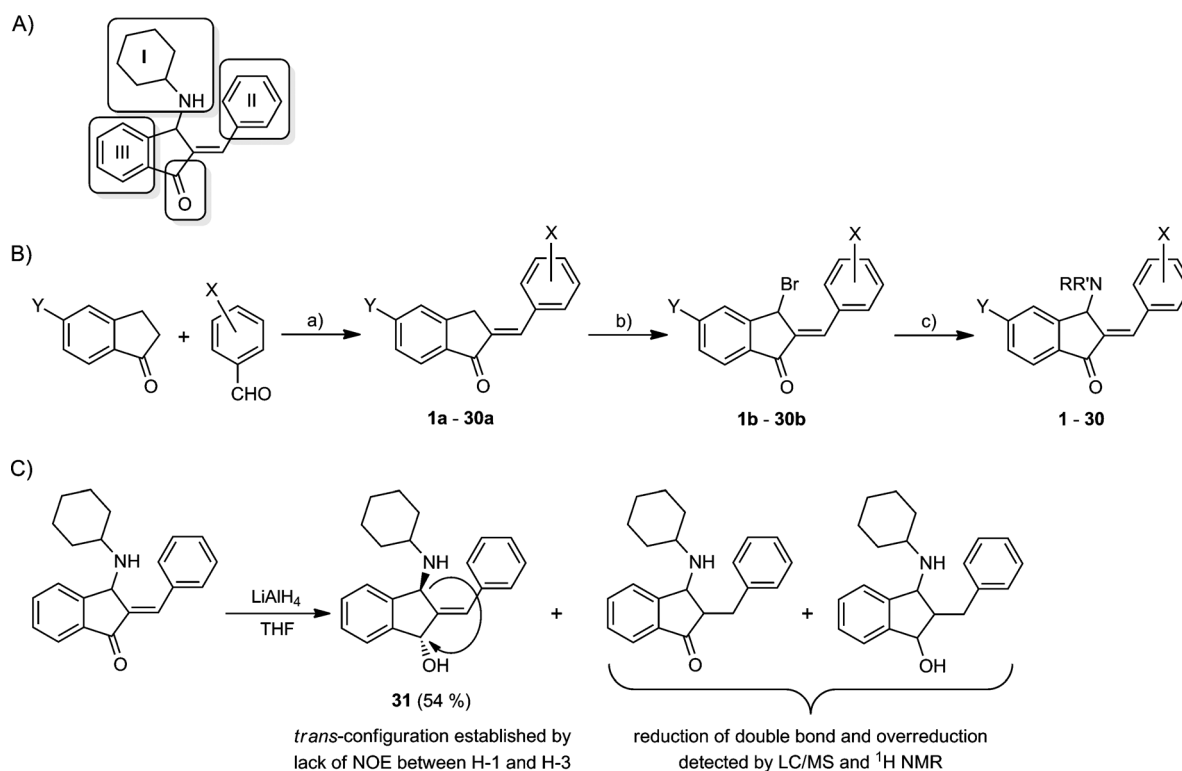
### Chemical synthesis of BCI analogues

Compound **1** has four distinct potential sites of modification (amine I, aromatic rings II and III, and the carbonyl group, Scheme 1A). We created a small library of 29 analogues, designed to probe spatial and hydrogen bonding requirements of the aminoalkyl (ring I) system (compounds **2–11**, Table S1 in the Supporting Information) to modulate the electrophilicity

and hydrogen acceptor properties of the  $\alpha,\beta$ -unsaturated ketone through electron-donating or electron-withdrawing substituents in rings II and III (Table S1, compounds **12–20**) and to investigate whether combinations of multiple structural modifications would reach maximal potency (Table S1, compounds **21–30**).

A convenient and flexible route to **1** and its analogues is shown in Scheme 1B. This route allowed synthesis of the parent compound and a series of analogues with a modified fragment I in Scheme 1A. The condensation of 5-substituted 1-indanones with appropriate benzaldehydes afforded the corresponding 2-benzylidene-1-indanones in quantitative yield. The bromination of 2-benzylidene-1-indanones with *N*-bromosuccinimide (NBS) provided 3-bromo-2-benzylidene-1-indanones.<sup>[22]</sup> The final synthetic step was the reaction of the 3-bromo-2-benzylidene-1-indanones with amines, as developed by Cromwell.<sup>[23]</sup> Reaction of unsubstituted 3-bromo-2-benzylidene-1-indanone (**1b**, X, Y=H) with amines proceeded in two steps, initially giving a 2-[ $\alpha$ -(alkylamino)benzyl]-1-indenone, which rearranged to the more thermodynamically stable 2-benzylidene-3-(alkylamino)-2,3-dihydro-1*H*-inden-1-one.<sup>[23]</sup>

The amine in position I was modified to examine steric effects, hydrogen-donating properties, effects of relative basicity of the amino group, and effects of introduction of additional hydrogen donors and acceptors. 3-Bromo-2-benzylidene-1-indanone (**1b**) was converted to analogues **1–11** by treatment with two equivalents of the corresponding primary or secondary amines in benzene at room temperature (Tables S2 and S3). The reaction provided the desired compounds in generally



**Scheme 1.** Design and generation of **1** and analogues. A) Sites of modification of the scaffold. B) Synthesis of **1** and its analogues. a) KOH, RT, or, AcOH,  $\text{H}_2\text{SO}_4$  (cat), RT; b) NBS,  $(\text{PhCO})_2\text{O}$ ,  $\text{CCl}_4$ , reflux; c)  $\text{RR}'\text{NH}$  (2 equiv),  $\text{C}_6\text{H}_6$ , RT. C) Synthesis of aminoalcohol **31**.

high yield; one notable exception was the 4-piperazine analogue (**9**, BCI-187), which was afforded in 42% yield when using 1.9 equivalents of piperazine. Using two equivalents of piperazine resulted in formation of a mixture of the desired compound and isomerization products with migration of the piperazine group. Maury et al. reported that **1** and analogues are labile compounds that can undergo allylic rearrangements with migration of the amino group or prototropic isomerization of the double bond into an endocyclic alkene.<sup>[23]</sup> The rate of this isomerization is dependent on the nature of the amine, but formation of the desired product was complete in our hands within 24 h; the one exception was the reaction of **1b** with aniline, which required 120 h and provided compound **4** (BCI-11) in 69% yield.

This method was found to be suitable for the synthesis of analogues containing additional substituents in rings II or III, as well as analogues containing combinations of different amines in position I. Acid- or base-catalyzed condensation of substituted benzaldehydes or indanones in the first step provided corresponding 2-arylideneindan-1-ones **12a–30a** in good yield.<sup>[24]</sup> Following bromination with NBS, treatment of the resulting 3-bromo-2-arylideneindan-1-ones **12b–30b** with cyclohexylamine in benzene provided final products bearing substituents in rings II (12–17), III (18–20), and II and III (21, 22). Compounds **23–30** were synthesized as described above using morpholine.

To probe the importance of the carbonyl group, we also synthesized 2-benzylidene-3-cyclohexylaminoindan-1-ol (**31**, BCI-10), with a *trans* relationship between the amine and hydroxy groups (as documented by the absence of a nuclear Overhauser effect (NOE) between H-1 and H-3) through the reduction of **1** with LiAlH<sub>4</sub> (Scheme 1C). The moderate yield of alcohol **31** was attributed to over-reduction of both the carbonyl group and the carbon–carbon double bond.

### Structure–activity studies in zebrafish embryos

We first analyzed all analogues for hyperactivation of FGF signaling in the *Tg(dusp6:EGFP)<sup>pt6</sup>* transgenic zebrafish model. In this assay, we previously established transgenic zebrafish that express destabilized GFP under the control of active FGF signaling.<sup>[11,12]</sup> These transgenic embryos respond to FGF activation with GFP expression in specific areas of the brain, which can be quantified by automated image analysis using cognition network technology (CNT).<sup>[25]</sup> To determine optimal conditions for FGF reporter activation, and to test whether the response was saturable, we performed time- and concentration-dependence experiments. Twenty-four hours post-fertilization (hpf), embryos were treated with 20 μM of **1**, and images were acquired as described

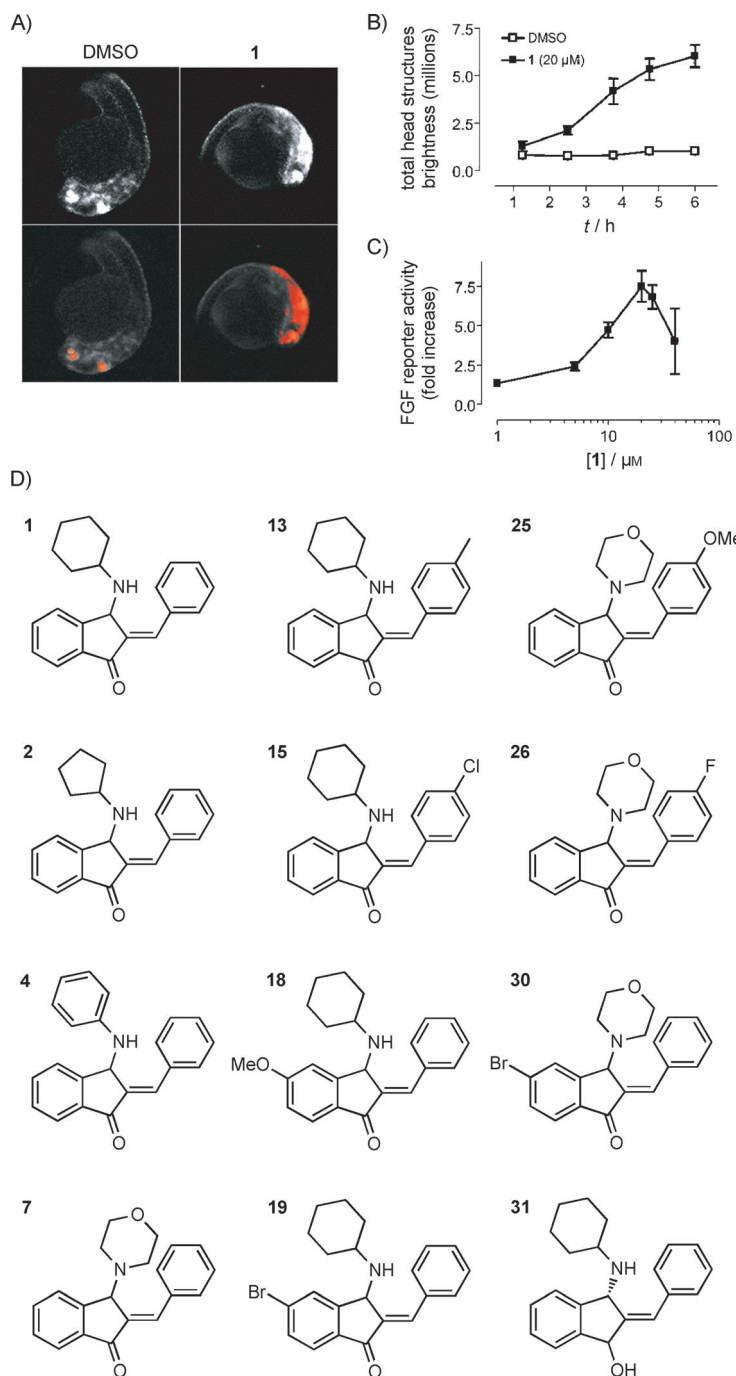


**Figure 1.** Quantitation of in vivo FGF hyperactivation by automated image analysis. A) Upper panel. Representative fluorescence micrographs of 24 hpf *Tg(dusp6:EGFP)<sup>pt6</sup>* embryos treated for 5 h with vehicle (1% DMSO) or 20 μM **1**. The major bright head structures are eye and retina, mid-hindbrain boundary, and trigeminal ganglia. Lower panel. Archived scan images with CNT algorithm applied. Areas in red are regions of GFP expression in the head that exceeded a threshold relative to yolk sac fluorescence. B) Time course of FGF activation. After 24 hpf, *Tg(dusp6:EGFP)<sup>pt6</sup>* embryos were exposed to vehicle (DMSO) or 20 μM **1** in 96-well plates, imaged every hour for 6 h, and analyzed by the CNT rule set. Data show total GFP intensity in the head from eight embryos per condition ± SEM. C) Dose–response of FGF activation by **1** at 5 h after treatment. D) Chemical structures of important BCI analogues and numbering scheme used in this study.

previously.<sup>[25,26]</sup> Figure 1A shows representative fluorescence micrographs of vehicle- or **1**-treated embryos before and after CNT analysis.<sup>[26]</sup> Time course experiments in embryos treated

with **1** showed that after 5 h, GFP expression reached a maximum and remained stable for an additional hour (Figure 1B). A concentration-dependence experiment at the 5 h time point documented that FGF reporter activation was maximal at 20  $\mu\text{M}$  and declined at higher concentrations (Figure 1C). We tested all 29 analogues to determine if any of the new compounds induced GFP expression similar to **1** (Table S4). Dose-response curves were obtained, showing that nine compounds were equipotent to **1**, and one agent, **7** (BCI-9), had significantly higher activity than **1** ( $\text{EC}_{50}=4.5 \mu\text{M}$ ) (Table 1). In total, in

The pharmacophore of **1** contains an electrophilic  $\alpha,\beta$ -unsaturated ketone moiety, and although many marketed drugs are electrophilic, the presence of such elements is often viewed as a liability in drug development, due to possible non-selective modification of cellular nucleophiles, leading to off-target effects and toxicity. Indeed, many of the active agents at the highest doses started to show whole organism toxicity at the time of imaging, as manifested by gross morphological changes (data not shown). We therefore assessed toxicity upon prolonged exposure to agents (24 h) by visual inspection

of larvae for morphological changes, such as a bent tail phenotype and the appearance of opaque, necrotic cells (Figure 2; Tables S4 and S5). Cellular toxicity was confirmed by staining with acridine orange (a vital dye that labels cells with damaged cell membranes), revealing the presence of dead cells in the tail (data not shown).

Several agents exhibited little or no toxicity at concentrations that hyperactivated FGF signaling in vivo (Tables S4 and S5). Conversely, we found some agents that did not hyperactivate FGF signaling but caused developmental toxicity, and several that were devoid of toxicity and activity, including alcohol **31** (Tables S4 and S5 and Figure 2). The latter observation suggests that, although the  $\alpha,\beta$ -unsaturated ketone moiety is important for FGF hyperactivation, it also

could also be a contributing factor in embryo toxicity. To further explore this hypothesis, we examined whether there was a correlation between toxicity and electrophilicity by calculating Hammett  $\sigma$  constants for **1** and nine analogues with or without in vivo FGF enhancing activity. Hammett  $\sigma$  constants ranged from  $-0.54$  (low electrophilicity) to  $0.60$  (high electrophilicity), covering the entire spectrum of chemical reactivities in the series (Figure 2).

At concentrations at or above their  $\text{EC}_{50}$  values (5–10  $\mu\text{M}$ ), analogues with negative Hammett  $\sigma$  values (lower electrophilicity) showed toxicity (Figure 2). In contrast, compounds with positive Hammett  $\sigma$  values appeared to be less toxic. Thus, surprisingly, agents with predicted high electrophilicity were generally better tolerated. There seemed to be no correlation between toxicity and in vivo target activity, as two inactive analogues (**21** (BCI-266) and **24** (BCI-256)) were also toxic. Collectively, the data demonstrate that electrophilicity does not significantly contribute to toxicity. This suggests that, although the unsaturated ketone is required for activity, it does not indiscriminately modify essential cellular constituents, and that the untoward effects of compounds are due to off-target ef-

**Table 1.** Activity of BCI analogues.

Compound	Alias	FGF reporter activation in zebrafish $\text{EC}_{50}$ [ $\mu\text{M}$ ]	$p$	Cellular inhibition of DUSP6	Cellular inhibition of DUSP1
<b>1</b>	BCI	$10.6 \pm 0.8$ (14)		$13.3 \pm 1.8$ (12)	$8.0 \pm 0.6$ (11)
<b>2</b>	BCI-164	$13.3 \pm 3.3$ (2)	0.56	$15.8 \pm 3.0$ (3)	$8.3 \pm 0.8$ (3)
<b>3</b>	BCI-165	$12.3 \pm 0.8$ (2)	0.21	$25.0 \pm 7.0$ (3)	$14.0 \pm 2.8$ (3)
<b>4</b>	BCI-11	$\geq 25$		n.d.	n.d.
<b>5</b>	BCI-8	$13.6$ (1)		n.d.	n.d.
<b>7</b>	BCI-9	$4.5 \pm 0.6$ (7)	$\leq 0.01$	$50.8 \pm 4.1$ (7)	$28.4 \pm 1.8$ (6)
<b>12</b>	BCI-211	$22.6 \pm 2.6$ (3)	0.04	n.d.	n.d.
<b>13</b>	BCI-212	$12.0 \pm 1.5$ (5)	0.47	$64.7 \pm 15.7$ (3)	$25.5 \pm 6.1$ (3)
<b>14</b>	BCI-303	$8.9 \pm 2.5$ (2)	0.6	n.d.	n.d.
<b>15</b>	BCI-183	$10.0 \pm 1.1$ (4)	0.66	$37.8 \pm 11.8$ (3)	$14.7 \pm 4.4$ (3)
<b>16</b>	BCI-297	$\sim 10.0$ (1)		n.d.	n.d.
<b>18</b>	BCI-216	$10.4 \pm 0.6$ (3)	0.81	$67.8 \pm 14.2$ (3)	$28.0 \pm 5.0$ (3)
<b>19</b>	BCI-215	$12.0 \pm 3.0$ (6)	0.67	$55.9 \pm 8.6$ (9)	$28.6 \pm 3.8$ (11)
<b>24</b>	BCI-256	$\geq 25$		$\geq 100$ (2)	$\geq 100$ (2)
<b>25</b>	BCI-269	$7.1 \pm 0.7$ (2)	0.02	n.d.	n.d.
<b>26</b>	BCI-304	$10.3$ (2)		n.d.	n.d.
<b>28</b>	BCI-296	$\geq 25$		$\geq 100$ (2)	$\geq 100$ (2)
<b>30</b>	BCI-299	$\geq 25$		n.d.	n.d.
<b>31</b>	BCI-10	$\geq 25$		n.d.	n.d.

Average  $\text{EC}_{50} \pm \text{S.E.}$  of  $n$  experiments.  $p$  value: compared with BCI by Student's  $t$ -test (two tailed, unequal variances). n.d.: not determined.

vivo SAR identified 11 new compounds that showed concentration-dependent hyperactivation of FGF signaling in *Tg(dusp6:EGFP)<sup>pt6</sup>* embryos (Table 1, relevant structures shown in Figure 1D). Structural elements essential for activity included an aliphatic amino-alkyl side chain at C-3 and the  $\alpha,\beta$ -unsaturated ketone moiety. Changes that were tolerated without loss of activity were moderately electron-donating or -withdrawing substituents in rings II and III. A planar aromatic amine in ring I and a strongly electron-withdrawing cyano substituent in rings II or III were not tolerated (see Discussion for more details). These data document that specific structural modifications affected biological activity, suggesting that **1** is a bona fide pharmacophore of in vivo FGF signaling.

#### Identification of a non-toxic analogue of **1** with cellular and in vivo activity

Because the primary assay for biological activity involved the use of a living vertebrate animal, we were able to observe whole organism toxicities upon compound treatment and to relate toxicity to in vivo target activity and chemical reactivity.

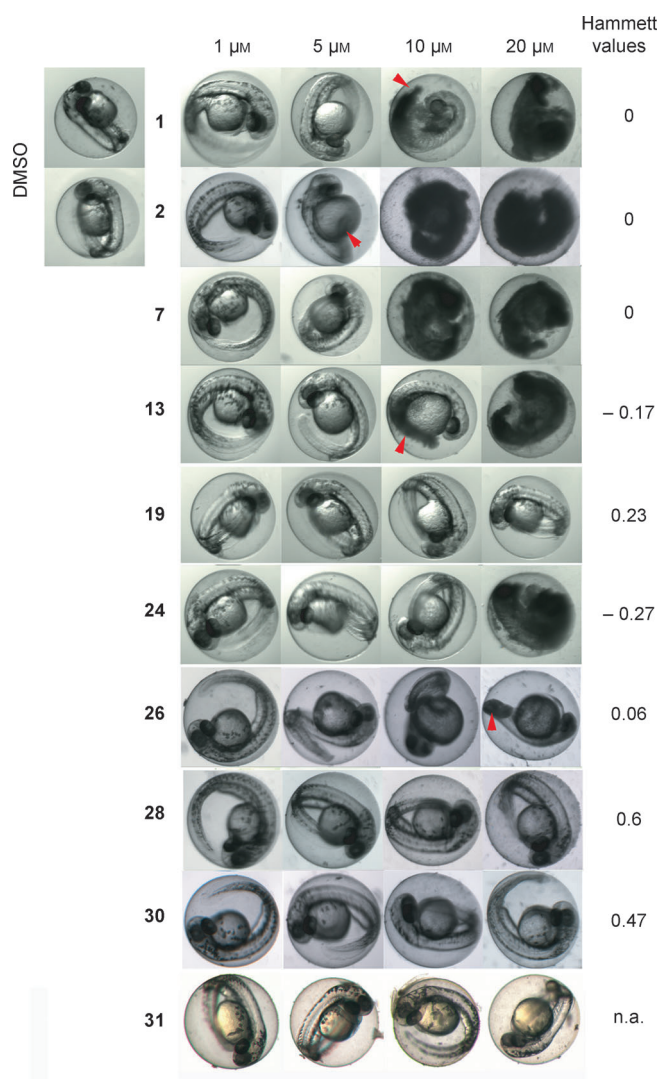


**Figure 2.** Compound **19** lacks whole organism toxicity. Images show transmitted light micrographs of embryos in the presence of vehicle (DMSO), or the indicated concentrations of test agents after 24 h of treatment. Toxicity manifests itself by the appearance of opaque cells, indicating necrosis (red arrows demarcate examples of necrotic cells). Compound **19**, **27**, and **29**, **30** exhibited minimal toxicity. Hammett  $\sigma$  values indicate the degree of electrophilicity of the  $\alpha,\beta$ -unsaturated ketone moiety.

ffects unrelated to chemical reactivity. One agent in particular, compound **19** (BCI-215), did not show any toxicity at concentrations two times higher than the  $EC_{50}$  value for FGF activation (Figure 2). To probe for possible developmental delays or defects, we performed a hatching study and found that larvae treated with **19** developed normally. After a 6 h exposure followed by a washout, 100% of vehicle- or compound **19**-treated embryos, at a concentration two times higher than the  $EC_{50}$  for FGF activation ( $20 \mu\text{M}$ ), had hatched by 56 hpf (data not shown). In contrast, no embryos hatched after exposure to **1** or **7** at their  $EC_{50}$  concentrations ( $10$  or  $5 \mu\text{M}$ , respectively). Thus, **19** lacked whole organism toxicity at concentrations that activated FGF signaling. To corroborate the results from the zebrafish developmental toxicity studies, we performed a cytotox-

icity experiment in EA.hy926 cells, a hybridoma cell line that retains many properties of normal endothelial cells.<sup>[27–29]</sup> Although both agents were relatively non-toxic under the conditions of the assay, BCI showed signs of cell loss, nuclear condensation, and necrosis (PI staining) at concentrations above  $25 \mu\text{M}$  (Figure S1). In contrast, BCI-215 was devoid of cellular toxicity at concentrations up to  $50 \mu\text{M}$  (Figure S1). Therefore, the cellular assay recapitulated differences in developmental toxicity.

### Analogues of **1** inhibit DUSPs in a chemical complementation assay

To test whether the FGF-hyperactivating activities of the new analogues were due to DUSP inhibition, we tested seven agents that had shown robust activity in zebrafish and that were available in sufficient quantities for DUSP6 and DUSP1 inhibitory activity in our mammalian cell-based chemical complementation assay (Table 1).<sup>[30]</sup> In this assay, HeLa cells were transfected with Myc-tagged DUSP1 or DUSP6 and stimulated with phorbol ester (TPA) to activate the ERK pathway. The expression of active phosphatases in the assay decreases TPA-induced ERK phosphorylation. Thus, compounds that inhibit DUSP activity restore pERK levels in DUSP-overexpressing cells. Restoration of ERK phosphorylation can be quantified by comparing pERK distributions of treated and untreated cell populations by Kolmogorov–Smirnov (KS) statistics. Figure 3A shows that **1**, **7**, and **19** increased pERK levels in DUSP-overexpressing cells in a concentration-dependent manner, with  $IC_{50}$  values in the micromolar range. Figure 3B shows representative images for **19** that illustrate restoration of ERK phosphorylation in DUSP-overexpressing cells. Table 1 shows that all agents with activity in zebrafish also inhibited DUSP6 and DUSP1 in mammalian cells, whereas two inactive compounds (**24** (BCI-256) and **28** (BCI-296)) lacked antiphosphatase activity. Hence, these data support the hypothesis that *in vivo* activity of the analogues is due to DUSP inactivation and validate the core structure of **1** as a pharmacophore for DUSP inhibition.

### Analogues of **1** suppress ERK-stimulated activation of DUSP6

DUSP6 activity is stimulated upon substrate binding. In the absence of ERK, DUSP6 has low basal catalytic activity, which is significantly enhanced upon interaction with ERK.<sup>[15]</sup> *In vitro* studies with **1** suggested that its mechanism of action involved suppressing this ERK-stimulated activation of DUSP6.<sup>[13]</sup> We confirmed that analogues of **1** also inhibited the activation of DUSP6 by ERK binding (Figure 4A and B). Compounds **1**, **7**, and **19** significantly suppressed activation of DUSP6 with similar magnitudes (Figure 4A and B). Consistent with previous data,<sup>[13]</sup> none of the tested agents inhibited basal phosphatase activity (Figure 4A). In contrast, suppression of DUSP6 activation by compound **31**, which failed to hyperactivate FGF signaling in the transgenic embryos, was insignificant (Figure 4A and B). Thus, *in vitro* inhibition of DUSP6 by analogues of **1** correlated with *in vivo* activity.

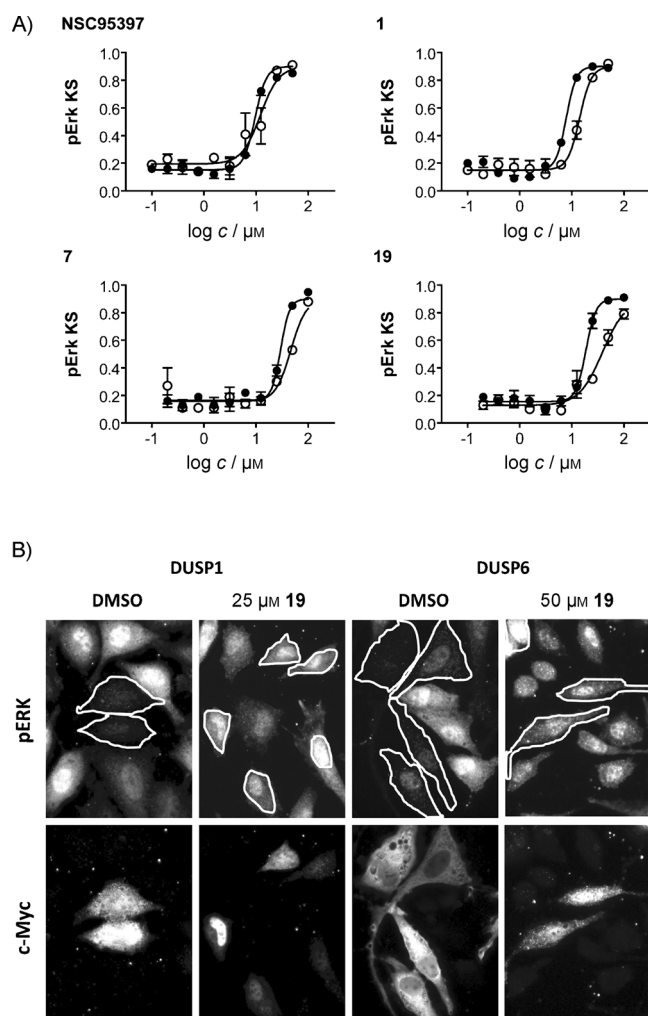


**Figure 3.** Inhibition of DUSP6 and DUSP1 by analogues of compound **1** in mammalian cells. A) Concentration-dependent inhibition of DUSP1 (closed symbols) and DUSP6 (open symbols) by **1** and analogues and a previously described multi-targeted DUSP inhibitor (NSC95397). B) Representative fluorescence micrographs of ERK phosphorylation (upper panel) and DUSP expression (lower panel) in the presence or absence of compound **19**. Restoration of ERK phosphorylation in DUSP-expressing cells is observed after treatment with **19**.

### Refinement of the DUSP6-1 binding model by computational modeling and simulation

We previously established the necessity of both the cyclohexylamino substituent and the benzylidene substituent for the biological activity of compound **1**.<sup>[13]</sup> These experimental findings were consistent with a computational model of **1** binding to an allosteric site on DUSP6 in an orientation in which both rings make contact with the interior of the pocket through hydrophobic interactions. Occupation of this site by **1** is thought to prevent a conformational change in DUSP6, which otherwise would accommodate ERK binding upon positioning Asp262 (in the general acid loop, GAL) close to Arg299 of the phosphatase catalytic site (Figure 4C and Movie S1).<sup>[31]</sup> The ensemble docking and clustering approach that we previously utilized identified multiple potential orientations for **1** in the allosteric pocket with comparable interaction scores.<sup>[13]</sup> The scoring incorporated only pairwise atomic interactions as a weight-

ed sum of van der Waals interactions and hydrogen bond formation energies. The allosteric pocket of DUSP6, however, features charged Asp262 and Arg299 side chains and hydrophobic patches, the interactions of which were not accounted for in the pairwise atomic interactions. Hence, we rigorously evaluated electrostatic and solvation effects to gain insights that would complement the SAR studies. To this end, we refined the structural model of the DUSP6-1 interaction by rescoring docking modes with the help of PBSA calculations implemented in the *FRED* application (OpenEye, Santa Fe, NM).<sup>[32]</sup> PB and SA components of this scoring method describe electrostatic interactions and solvation effects, respectively. The method is computationally more expensive than force-field-based scoring, and hence, is generally applied for refinement in post-processing of docking poses.<sup>[33]</sup>

Application of this method permitted us to prioritize the binding pose of **1** shown in Figure 4C and D. Consistent with the existing model and the fact that deletion of the benzylidene moiety abolishes biological activity,<sup>[13]</sup> the refined model showed the indanone ring buried deep in the binding pocket. Two previously undetected hydrogen bonds were observed by using molecular dynamics simulations starting from this docking pose (Movie S2): the first between the ketone oxygen of **1** and the Arg299 side chain, and the second between the secondary amine of the cyclohexylamino side chain of **1** and the Trp264 backbone oxygen. In addition, Trp264 makes hydrophobic contacts with the aminocyclohexane moiety. To confirm these computational predictions, we analyzed docking of **31** to DUSP6 by using the same parameters as DUSP6-1 (Figure 4E). No hydrogen bond formation was observed between Arg299 and the  $\alpha,\beta$ -unsaturated alcohol moiety in **31**, in support of a model where the  $\alpha,\beta$ -unsaturated ketone moiety in **1** is required for DUSP6 inhibition through hydrogen bonding but not covalent modification, consistent with experimental observations.

## Discussion and Conclusions

Despite the evidence that DUSPs play important roles in a variety of maladies, including cancer,<sup>[34]</sup> inflammation,<sup>[35]</sup> and immune dysfunction,<sup>[16]</sup> they have largely eluded attempts to discover biologically active small molecule inhibitors. The reasons for this are numerous and include overlapping substrate specificity, shallow and feature-poor active sites, redox sensitivity, and the use of *in vitro* assays that do not represent the activity of these enzymes within their biological context. We recently identified a small molecule, compound **1**, which inhibits the activation of DUSP6 by ERK and presumably binds to a novel allosteric site on DUSP6. In this report, we designed a series of novel analogues of **1** to explore their SARs through *in vivo* studies using transgenic zebrafish, with confirmation by an *in vitro* phosphatase assay.

### *In vivo* SAR supports the importance of:

*Ring I*: Changing the size of the aliphatic ring I in analogues **2** (BCI-164) and **3** (BCI-165) preserved activity, whereas replace-

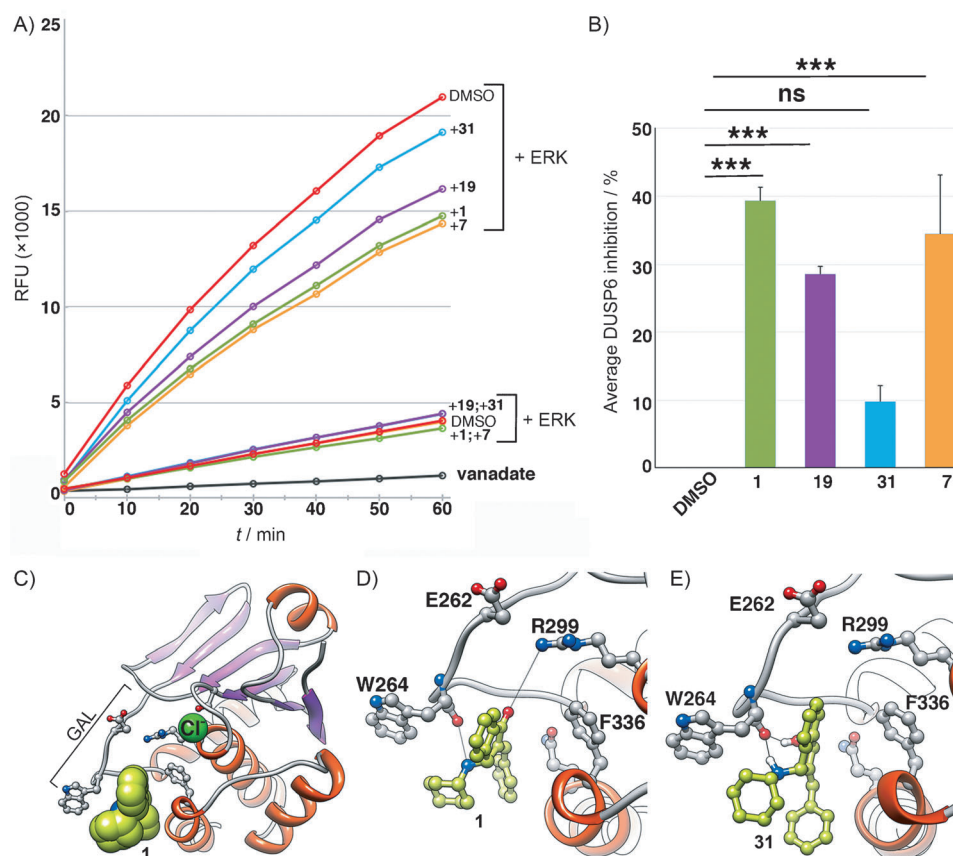


**Figure 4.** Compounds **1**, **7**, and **19** inhibit ERK2-stimulated activation of DUSP6 catalytic activity in vitro. A) DUSP6 phosphatase activity in the presence and absence of ERK2. Inclusion of **1**, **7** and **19** partially suppressed DUSP6 activation by ERK2 but not basal phosphatase activity. In contrast, compound **31** showed only a minor effect. Data are from a single experiment that has been repeated twice with identical results. Vanadate was used as a positive control. Note that in assays in the absence of ERK, results from treatment with **1** overlapped with **7** and **19** with **31**. B) Graph showing average percent inhibition of DUSP6 hyperactivation  $\pm$  SD from three independent experiments by **1**, **7**, **31** and **19**. Percent inhibition was graphed from results at 10 min when the assay was within the linear range. \*\*\*,  $p < 0.001$  by one-way ANOVA compared with vehicle control. C) Overview of putative allosteric binding site of **1** and docking orientation (chloride ion highlights catalytic site). D) Close-up view of **1**'s interactions with allosteric binding site residues. Two hydrogen bonds are observed (black dotted lines), between the ketone oxygen of **1** and Arg299 and the amine of **1** and the Trp264 backbone oxygen. E) Close-up view of the interactions of **31** with allosteric binding site residues. Hydrogen bonding of the amine in **31** and the backbone oxygen of Trp264 is present. In contrast, hydrogen bonding with Arg299, as noted for **1**, is absent.

ment of the cyclohexyl ring with a phenyl ring in analogue **4** (BCI-11) abolished activity (Table 1). Shortening the side chain by incorporating the nitrogen into the aliphatic ring preserved activity (compound **5** (BCI-8)). Introduction of heteroatoms into ring I abolished activity (analogues **8–11**). A notable exception appeared to be the morpholine-substituted compound **7**, which had the maximal in vivo activity among all tested BCI analogues.

**Rings II and III:** Substituents at the *para* position in ring II with electron-donating (OMe: **12** (BCI-211), Me: **13** (BCI-212)) or electron-withdrawing (F: **14** (BCI-303), Cl: **15** (BCI-183), 3,4-Cl<sub>2</sub>: **16** (BCI-297)) groups did not exhibit substantial changes in activity compared to **1** (Table 1). The strongest electron-withdrawing cyano group (compound **17** (BCI-7)), however, was not tolerated. Similar results were obtained for compounds with substitutions in ring III (compounds **18–20**), where methoxy (compound **18** (BCI-216)) and bromo (compound **19** (BCI-

**215**)) substituents were tolerated, but a cyano group was not (compound **20** (BCI-169)). Finally, reduction of the  $\alpha,\beta$ -unsaturated ketone to the  $\alpha,\beta$ -unsaturated alcohol (compound **31**, Scheme 1C) abolished activity. These results are consistent with the prediction by the model that the carbonyl group of the indanone system engaged in a hydrogen bond with Arg299, with a minor contribution from an additional hydrogen bond between the cyclohexylamino moiety and Trp264.

### Double substitutions and combination with a morpholino substituent in ring I

Simultaneous substitutions in both rings II and III with methoxy groups or halogens rendered the scaffold inactive (**21**, **22** (BCI-283)). Because of the unique ability of the morpholino substituent in ring I to increase potency (analogue **7**), we investigated whether inclusion of a morpholino moiety in the ring I position, along with substituents in rings II and III would improve the activity; this hypothesis was not supported. Although the activity of a fluoro-substituted compound was preserved (**14** vs. **26** (BCI-304)), the replacement of cyclohexylamine with morpholine did not render previously inactive compounds active (**21** vs. **23** (BCI-267), **22** vs. **29** (BCI-282)). Furthermore, the morpholino substituent abolished the activity of three active agents (analogues **24**, **27** (BCI-271), and **28** (BCI-296)). Thus, the ability of the morpholino group to preserve or improve potency was limited to unsubstituted (**7**) and *para*-fluoro-substituted (**26**) analogues.

### In vivo activity and DUSP inhibition

There is considerable debate regarding whether potent and selective inhibitors of DUSPs can be obtained. Multiple attempts at discovering DUSP inhibitors have failed, and because adequate probes are lacking, the question of what degree of specificity is required to elicit desired biological responses has been intractable. The dearth of chemical probes for DUSP activity has also prevented proof-of-principle studies in mammals. Our studies demonstrate that DUSPs might be druggable

through exploitation of allosteric mechanisms. First, compound **1** and seven analogues that activated FGF signaling in vivo also inhibited mammalian DUSP1 and DUSP6 in cultured cells, whereas agents that lacked in vivo activity were devoid of anti-phosphatase activity. This is a significant finding as, prior to our current studies, only three agents had ever shown confirmed activity in the mammalian cell-based chemical complementation assay, namely the thiol poison, phenyl arsine oxide,<sup>[36]</sup> the glutathione-depleting alkaloid, sanguinarine,<sup>[30]</sup> and the *para*-quinone, NSC95397.<sup>[37]</sup> Second, experimental data were consistent with computational modeling predictions based on the DUSP6–1 interactions at the allosteric site, lending credence to the proposed mechanism of inhibition. Taken together, the results validate the **1** scaffold as a bona fide pharmacophore for allosteric DUSP6 inhibition.

All agents with in vivo activity were inhibitors of both DUSP6 and DUSP1. Because there is no published X-ray crystal structure of DUSP1, we created a homology model and showed that the allosteric site also exists on DUSP1 (data not shown). Therefore, the pharmacophore of **1** might not be expected to show selectivity for either DUSP.

Although we observed a correlation between in vivo and cellular activity, there were differences in potency between these assays. The most likely reasons for this are solubility, uptake, and/or protein binding, as zebrafish assays are performed in an unbuffered aqueous solution, whereas cellular assays are conducted in complete growth medium with serum. The most striking difference between assays was observed in the in vitro DUSP hyperactivation assay, where compounds showed only partial activity at high concentrations (100  $\mu\text{M}$ ). Although we have observed this phenomenon before,<sup>[13]</sup> a definitive explanation is lacking. One reason for the lack of in vitro activity could be that multiple binding processes and enzymatic reactions with different affinities and kinetics occur concurrently, possibly affecting the enzyme–inhibitor interaction. Alternatively, in vitro assays might not faithfully represent biological conditions, due to lack of a proper microenvironment and accessory/scaffolding proteins.

Neither the dual inhibitory nature of **1** and analogues nor the presence of an electrophilic  $\alpha,\beta$ -unsaturated ketone appeared to influence FGF hyperactivation. More importantly, the fact that embryos treated with compound **19** developed normally suggests that neither a lack of selectivity nor the presence of a potentially electrophilic moiety were causes for toxicity. These features make compound **19** not only an attractive candidate for further evaluation in mammals but also provide the research community with a much cleaner probe than **1** to investigate the biological functions of DUSP1 and DUSP6. The data demonstrate the rich potential of zebrafish in early drug discovery and identify compound **19** as a candidate for proof-of-principle studies to investigate the role of DUSP6 in embryonic development and disease models.

DUSPs have long eluded drug discovery efforts using the contemporary single-target, biochemical assay-based discovery paradigm. Their active sites are shallow, and their catalytic activity depends on a highly reactive, redox-sensitive cysteine. Prior discovery efforts, therefore, have been exceedingly good

at discovering redox-active, nonselective inhibitors with lack of or promiscuous cellular activity. Our findings suggest that targeting DUSPs by allosteric mechanisms can circumvent many of the problems caused by the nature of DUSP's catalytic cavity. The zebrafish in particular has been indispensable in discovering such inhibitors, and the present data create continued enthusiasm for the further identification of DUSP inhibitors by phenotypic discovery in transgenic zebrafish.

## Experimental Section

**Chemical synthesis:** The synthesis of and analytical data for all compounds are described in the Supporting Information.

**Zebrafish maintenance and compound treatment:** All procedures involving zebrafish were reviewed and approved by the University of Pittsburgh Institutional Animal Care and Use Committee. *Tg(dusp6:eGFP)<sup>pt6</sup>* embryos were obtained by natural mating and incubated at 28.5 °C.<sup>[26]</sup> One transgenic embryo was placed into every well of a 96-well plate in E3 (200  $\mu\text{L}$ ; 5 mM NaCl, 0.17 mM KCl, 0.33 mM CaCl<sub>2</sub>, 0.33 mM MgSO<sub>4</sub>). Compounds were dissolved as 100 $\times$  stock solutions in DMSO, and aliquots (2  $\mu\text{L}$ ) of each were added directly to octuplicate wells. For the SAR studies, a negative control (8 wells of DMSO (1%)) was included on every plate. A full dose–response for **1** was run on each day of experiments.

**Automated imaging and analysis:** At the end of compound treatment, embryos were anesthetized with 40  $\mu\text{g mL}^{-1}$  tricaine methanesulfonate (MS222, Sigma) in E3. Plates were loaded into an ImageXpress Ultra high-content reader (Molecular Devices) and imaged by using a 4 $\times$  objective at excitation/emission wavelengths of 488/525 nm (GFP).<sup>[26]</sup> Archived scan images were uploaded into Developer (Definiens AG) and analyzed for GFP expression in the head by using a simplified version of our previously described CNT rule set.<sup>[26]</sup> A GFP threshold was set, based on well background fluorescence, and regions within the zebrafish larva were classified as positive for GFP expression if their fluorescence intensity exceeded this threshold. GFP-expressing areas were merged, and the four largest objects were selected for quantitation. [Total head structure brightness = (mean GFP intensity)  $\times$  (area of the four head structures)]. EC<sub>50</sub> values were determined from dose–response curves by a four-parameter logistic equation where the bottom and top were defined as the magnitude of FGF activation by 1% DMSO and by the maximum response elicited by the positive plate control (usually seen with 20  $\mu\text{M}$  of **1**), respectively. EC<sub>50</sub> values in Table 1 are the averages  $\pm$  SEM of *n* independent experiments.

**Developmental toxicity assessments:** After drug treatment and GFP quantitation, embryos in microplates were returned to the incubator overnight in the continued presence of test agents. After a total of 24 h treatment, wells were examined visually for signs of toxicity, such as changes in gross morphology, necrosis, heart beat, and circulation to tail. Selected larvae were photographed on a transmitted light microscope to document toxicity.

**Cell culture:** HeLa cells were obtained from ATCC (Manassas, VA) and were maintained in Dulbecco's modified Eagle's medium (DMEM) containing 10% fetal bovine serum (FBS; HyClone, Logan, UT), and 1% penicillin–streptomycin (Invitrogen) in a humidified atmosphere of 5% CO<sub>2</sub> at 37 °C. EA.hy926 cells (ATCC CRL-2922), a hybridoma cell line that retains many properties of normal endothelial cells,<sup>[27–29]</sup> were maintained in DMEM supplemented with

10% FBS, 100  $\mu\text{g mL}^{-1}$  penicillin–streptomycin, and 2 mM glutamine.

**Cytotoxicity of BCI analogues in cultured cells:** EA.hy926 cells (10000 cells per well) were plated in the wells of a 384-well microplate, allowed to attach overnight, and treated with five-point, 1/3 dose reduction gradients of **1** and **19**. The non-selective thiol poison phenylarsine oxide (PAO), which induces apoptosis in normal cells,<sup>[38]</sup> was included as a positive control. After 6 h of continuous exposure, cells were stained with 1  $\mu\text{g mL}^{-1}$  propidium iodide (PI) and 10  $\mu\text{g mL}^{-1}$  Hoechst 33342 to visualize necrotic cells and nuclei, respectively. Cells were imaged live on an ArrayScan II high-content reader. Numbers of nuclei per imaging field, nuclear condensation, and the percentage of PI-positive cells were determined by the target activation bioapplication as described.<sup>[38]</sup>

**Antibodies and plasmids:** Rabbit polyclonal phospho-ERK was from Cell Signaling Technology (Beverly, MA). Mouse monoclonal anti-c-myc (9E10) antibody was from Santa Cruz Biotechnology (Santa Cruz, CA). Secondary antibodies were Alexa Fluor 488-conjugated goat anti-mouse and Alexa Fluor 594-conjugated goat anti-rabbit (Invitrogen). c-Myc-DUSP6/MKP3 (PYST1) was in pSG5.<sup>[39,40]</sup> c-Myc-DUSP1-pcDNA3.1 was subcloned from a pET15b vector encoding DUSP1/MKP1/CL100 into pcDNA3.1 (both original plasmids were gifts from Steve Keyse, CRUK, Dundee).

**Chemical complementation assay for DUSP6 and DUSP1:** Compounds were analyzed for inhibition of DUSP1 and DUSP6 in intact cells as described.<sup>[13]</sup> Briefly, HeLa cells were transfected in 384-well plates with human c-Myc-DUSP6 or c-Myc-DUSP1 by using Fugene HD (Roche). After 48 h in culture, cells were treated in quadruplicate wells for 15 min with ten twofold concentration gradients of **1** and analogues or the nonselective DUSP inhibitor, NSC95397 (positive control), and stimulated for 15 min with phorbol ester (TPA, 500  $\text{ng mL}^{-1}$ ). Cells were immunostained with a mixture of anti-pERK (1:200 dilution) and anti-c-Myc (1:100 dilution) antibodies. Positive pERK and c-Myc-DUSP signals were visualized with Alexa Fluor 594 (pERK) and Alexa 488 (c-Myc) conjugated secondary antibodies, respectively. Plates were analyzed by three-channel multiparametric analysis for pERK and c-Myc-DUSP intensities in an area defined by nuclear staining by using the target activation bioapplication on the ArrayScan II (Thermo Fisher Cellomics, Pittsburgh, PA). DUSP transfected cells were classified as expressors if their average c-Myc staining intensity exceeded a threshold defined as the mean intensity + 2 SD of untransfected cells. pERK levels were quantified in the DUSP-expressing subpopulation by Kolmogorov-Smirnov statistics, comparing the cumulative pERK distribution of each test well to a reference distribution from 14 DUSP-transfected and vehicle-treated wells. High KS values denote large differences in ERK phosphorylation levels compared with vehicle control and indicate suppression of DUSP activity. KS values were plotted against compound concentration, and  $\text{IC}_{50}$  values were calculated by fitting curves to a four parameter logistic equation, with the top defined by the maximum KS value obtained in the presence of the highest concentration of the positive control (**1** or NSC95397).

**In vitro phosphatase assays:** 3-O-Methylfluorescein phosphate (OMFP)-based ERK2 induced activation of DUSP6 assays were performed as described.<sup>[13]</sup> Recombinant His-tagged Dusp6 was expressed from a bacterial expression vector and 250 ng were incubated with 100  $\mu\text{M}$  **1**, **7**, **19**, and **31**. To assay activated DUSP6, 210 ng of recombinant ERK2 (Cell Signaling Technology, Danvers, MA) was added to DUSP6/compound mixtures before the addition of OMFP (100  $\mu\text{M}$ ). The final reaction volume was 15  $\mu\text{L}$ . OMF fluo-

rescence was measured on an M5 multimode reader (Molecular Devices) at excitation/emission wavelengths of 485/525 nm at ten minute intervals for 1 h at room temperature.

**Statistical significance:** In vivo and cell-based assay data were analyzed by using the two-tailed Student's t-test, assuming unequal variances. For in vitro phosphatase activity assays, one-way ANOVA was performed between all groups, followed by post hoc comparison of means by using Tukeys multiple range test. *P* values of < 0.05 and < 0.001 were considered statistically significant for in vitro assays.

**Molecular modeling:** The scientific application FRED (OpenEye, Santa Fe, NM) was used for rescoring docking poses of **1** at the putative binding site in DUSP6 (PDB: 1MKP). AM1-BCC partial charges for **1** were calculated by using QUACPAC,<sup>[41]</sup> and conformers were generated by using OMEGA<sup>[42]</sup> with default options. Conformational changes in DUSP6 upon ERK binding (60 ns; Movie S1) and of the 1–DUSP6 complex (1.4 ns; Movie S2) were performed by using NAMD<sup>[43]</sup> and CHARMM force field using water simulations.<sup>[44]</sup>

**Movie S1: Dusp6 general acid loop motions:** The movie shows DUSP6 general acid loop (GAL) motions from an unbiased molecular dynamics simulation. Simulation was performed in the presence of water (not shown) by using PDB structure 1MKP. The GAL contains the catalytic residue Asp262, which is required for formation of the “catalytic triad” (with Cys293 and Arg299). Upon formation of the catalytic triad, DUSP6 performs its dephosphorylation function at a higher catalytic rate. This conformational shift is also referred to as the catalytic activation of DUSP6. The GAL in its active form from DUSP10 structure (PDB id: 1ZZW) is shown in yellow for comparison. Upon formation of the catalytic triad, Asp262 is shown in sphere representation.

**Movie S2: BCI and DUSP6 interactions:** The movie shows interactions of **1** in the allosteric pocket of DUSP6. Simulation was performed in the presence of water (not shown) by using PDB structure 1MKP. The bound conformation of **1** was obtained by molecular docking. Compound **1** buries its hydrophobic surface in the allosteric binding pocket and forms hydrogen bonds with Arg299 side-chain and Trp264 backbone oxygen. Hydrogen bond formation is indicated by blue dashed lines. Compound **1** binding in the allosteric pocket prevents a GAL movement that brings Asp262 into proximity with the catalytic cysteine (Cys293), thereby inhibiting catalytic activation of DUSP6.

## Abbreviations

BCI: (*E*)-2-benzylidene-3-(cyclohexylamino)-2,3-dihydro-1*H*-inden-1-one; CNT: cognition network technology; DUSP: dual specificity phosphatase;  $\text{EC}_{50}$ : Half-maximal effective concentration; FGF: fibroblast growth factor; FITC: fluorescein isothiocyanate; GAL: general acid loop; HBSS: Hank's balanced salt solution; HCS: high-content screening; hpf: hours post fertilization; MAPK: mitogen-activated protein kinase or MAP kinase; MKP3: MAP kinase phosphatase 3; NBS: *N*-bromosuccinimide; PBSA: Poisson–Boltzmann surface area; PDB: Protein Data Bank; PTP: protein tyrosine phosphatase; SAR: structure–activity relationship

## Acknowledgements

We thank Nina Senutovitch and Richard DeBiasio for technical assistance with the EA.hy926 cell line and Donna Huryn for critically reading the manuscript. Grants from the National Institutes

of Health supported this work [Grants R01 GM099738 and P41 GM103712 to I.B., CA78039 to A.V., HD053287 to M.T and A.V., and HL088016 to M.T.]. This project used the UPCI Chemical Biology Facility, supported in part by award NIH P30A047904. The content is solely the responsibility of the authors and does not necessarily represent the official views of the National Heart, Lung, and Blood Institute or the National Institutes of Health (NIH).

**Keywords:** BCI · cognition network technology · FGF signaling · high-content screening · zebrafish

- [1] A. Farooq, M. M. Zhou, *Cell. Signalling* **2004**, *16*, 769–779.
- [2] S. M. Keyse, *Curr. Opin. Cell Biol.* **2000**, *12*, 186–192.
- [3] K. I. Patterson, T. Brummer, P. M. O'Brien, R. J. Daly, *Biochem. J.* **2009**, *418*, 475–489.
- [4] Y. Kawakami, J. Rodriguez-Leon, C. M. Koth, D. Buscher, T. Itoh, A. Raya, J. K. Ng, C. R. Esteban, S. Takahashi, D. Henrique, M. F. Schwarz, H. Asahara, J. C. I. Belmonte, *Nat. Cell Biol.* **2003**, *5*, 513–519.
- [5] C. Li, D. A. Scott, E. Hatch, X. Tian, S. L. Mansour, *Development* **2007**, *134*, 167–176.
- [6] M. Tsang, S. Maegawa, A. Kiang, R. Habas, E. Weinberg, I. B. Dawid, *Development* **2004**, *131*, 2769–2779.
- [7] H. Kamata, S. Honda, S. Maeda, L. Chang, H. Hirata, M. Karin, *Cell* **2005**, *120*, 649–661.
- [8] M. Brisson, T. Nguyen, A. Vogt, J. Yalowich, A. Giorgianni, D. Tobi, I. Bahar, C. R. Stephenson, P. Wipf, J. S. Lazo, *Mol. Pharmacol.* **2004**, *66*, 824–833.
- [9] P. A. Johnston, C. A. Foster, T. Y. Shun, J. J. Skoko, S. Shinde, P. Wipf, J. S. Lazo, *Assay Drug Dev. Technol.* **2007**, *5*, 319–332.
- [10] K. Nemoto, A. Vogt, T. Oguri, J. S. Lazo, *Prostate* **2004**, *58*, 95–102.
- [11] G. A. Molina, S. C. Watkins, M. Tsang, *BMC Dev. Biol.* **2007**, *7*, 62.
- [12] M. Tsang, *Birth Defects Res. Part C* **2010**, *90*, 185–192.
- [13] G. Molina, A. Vogt, A. Bakan, W. Dai, P. Q. de Oliveira, W. Znosko, T. E. Smithgall, I. Bahar, J. S. Lazo, B. W. Day, M. Tsang, *Nat. Chem. Biol.* **2009**, *5*, 680–687.
- [14] J. S. Lazo, D. C. Aslan, E. C. Southwick, K. A. Cooley, A. P. Ducruet, B. Joo, A. Vogt, P. Wipf, *J. Med. Chem.* **2001**, *44*, 4042–4049.
- [15] M. Camps, A. Nichols, C. Gillieron, B. Antonsson, M. Muda, C. Chabert, U. Boschert, S. Arkininstall, *Science* **1998**, *280*, 1262–1265.
- [16] G. Li, M. Yu, W. W. Lee, M. Tsang, E. Krishnan, C. M. Weyand, J. J. Goronzy, *Nat. Med.* **2012**, *18*, 1518–1524.
- [17] M. Maillet, N. H. Purcell, M. A. Sargent, A. J. York, O. F. Bueno, J. D. Molkenkin, *J. Biol. Chem.* **2008**, *283*, 31246–31255.
- [18] M. Matsuda, D. D. Nogare, K. Somers, K. Martin, C. Wang, A. B. Chitnis, *Development* **2013**, *140*, 2387–2397.
- [19] Y. Niwa, H. Shimojo, A. Isomura, A. Gonzalez, H. Miyachi, R. Kageyama, *Genes Dev.* **2011**, *25*, 1115–1120.
- [20] F. C. Simoes, T. Peterkin, R. Patient, *Development* **2011**, *138*, 3235–3245.
- [21] J. R. Meyers, J. Planamento, P. Ebrum, N. Krulewitz, E. Wade, M. E. Pownall, *Dev. Biol.* **2013**, *378*, 107–121.
- [22] B. Pearson, R. Ayer, N. Cromwell, *J. Org. Chem.* **1962**, *27*, 3038–3044.
- [23] G. Maury, E. Wu, N. Cromwell, *J. Org. Chem.* **1968**, *33*, 1900–1907.
- [24] R. Murray, N. Cromwell, *J. Org. Chem.* **1976**, *41*, 3540–3545.
- [25] M. Saydmohammed, L. L. Vollmer, E. O. Onuoha, A. Vogt, M. Tsang, *Birth Defects Res. Part C* **2011**, *93*, 281–287.
- [26] A. Vogt, H. Codore, B. W. Day, N. A. Hukriede, M. Tsang, *J. Visualized. Exp.* **2010**, *40*, e1900.
- [27] C. J. Edgell, C. C. McDonald, J. B. Graham, *Proc. Natl. Acad. Sci. USA* **1983**, *80*, 3734–3737.
- [28] C. J. Edgell, J. E. Haizlip, C. R. Bagnell, J. P. Packenham, P. Harrison, B. Wilbourn, V. J. Madden, *In Vitro Cell. Dev. Biol.* **1990**, *26*, 1167–1172.
- [29] J. Bauer, M. Margolis, C. Schreiner, C. J. Edgell, J. Azizkhan, E. Lazarowski, R. L. Juliano, *J. Cell. Physiol.* **1992**, *153*, 437–449.
- [30] A. Vogt, J. S. Lazo, *Pharmacol. Ther.* **2005**, *107*, 212–221.
- [31] J. D. Rigas, R. H. Hoff, A. E. Rice, A. C. Hengge, J. M. Denu, *Biochemistry* **2001**, *40*, 4398–4406.
- [32] J. Grant, B. Pickup, A. Nicholls, *J. Comput. Chem.* **2001**, *22*, 608–640.
- [33] B. Kuhn, P. Gerber, T. Schulz-Gasch, M. Stahl, *J. Med. Chem.* **2005**, *48*, 4040–4048.
- [34] S. M. Keyse, *Cancer Metastasis Rev.* **2008**, *27*, 253–261.
- [35] Y. Liu, E. G. Shepherd, L. D. Nelin, *Nat. Rev. Immunol.* **2007**, *7*, 202–212.
- [36] A. Vogt, K. A. Cooley, M. Brisson, M. G. Tarpley, P. Wipf, J. S. Lazo, *Chem. Biol.* **2003**, *10*, 733–742.
- [37] A. Vogt, P. R. McDonald, A. Tamewitz, R. P. Sikorski, P. Wipf, J. J. Skoko III, J. S. Lazo, *Mol. Cancer Ther.* **2008**, *7*, 330–340.
- [38] A. Vogt, P. A. McPherson, X. Shen, R. Balachandran, G. Zhu, B. S. Raccor, S. G. Nelson, M. Tsang, B. W. Day, *Chem. Biol. Drug Des.* **2009**, *74*, 358–368.
- [39] S. Dowd, A. A. Sneddon, S. M. Keyse, *J. Cell Sci.* **1998**, *111*, 3389–3399.
- [40] L. A. Groom, A. A. Sneddon, D. R. Alessi, S. Dowd, S. M. Keyse, *EMBO J.* **1996**, *15*, 3621–3632.
- [41] A. Jakalian, D. B. Jack, C. I. Bayly, *J. Comput. Chem.* **2002**, *23*, 1623–1641.
- [42] J. Boström, J. R. Greenwood, J. Gottfries, *J. Mol. Graphics Modell.* **2003**, *21*, 449–462.
- [43] J. C. Phillips, R. Braun, W. Wang, J. Gumbart, E. Tajkhorshid, E. Villa, C. Chipot, R. D. Keel, L. Kale, K. Schulten, *J. Comput. Chem.* **2005**, *26*, 1781–1802.
- [44] K. Vanommeslaeghe, E. Hatcher, C. Acharya, S. Kundu, S. Zhong, J. Shim, E. Darian, O. Guvench, P. Lopes, I. Vorobyov, A. D. Mackerell, Jr., *J. Comput. Chem.* **2010**, *31*, 671–690.

Received: February 1, 2014

Published online on June 6, 2014